SUPPLEMENTARY INFORMATION

Plasmid construction - PPARγ wild type and F347A mutant were cloned into the pcDNA3.1 vector (Invitrogen, CA) and RXRαwas cloned into pCMX vector for cotransfection assay and *in vitro* transcription and translation. The synthesized three copies of DR1 element (5'-AAACTAGGTCAAAGGTCA-3', identical to the elements used in the crystallography studies) were cloned into luciferase reporter vector pTAL-Luc (Clontech, Mountain View, CA) via the *Mlu I* and *Bgl II* restriction sites.

Cell Culture and Cotransfections – CV-1 cells were cultured and transfected as previously described [1]. The day prior to cotransfection, cells were harvested and plated into 96-well tissue-culture plates at a density of 100,000 cells per well in 100 μl regular growth medium. The next day, cells were transfected with vectors directing the expression of either wild-type PPARγ or the PPARγ F347A mutant along with RXRα, the DR1 luciferase reporter, and a standard renilla luciferase reporter (pGL4.73, Promega, Madison, WI) used as control. Six hours post-transfection cells were treated with 1 μM rosiglitazone or DMSO control. Luciferase activity was measured using Dual-Glo™ Luciferase Assay System (Promega) after 24 hours treatment and all transfections were normalized to the renilla luciferase reporter. Expression of wild type and mutant PPARγ were equivalent as determined by a western blot. A single band was detected for both wild type and mutant PPARγ proteins using a specific PPARγ antibody (ab27450, Abcam, Cambridge, MA).

Electrophoretic Mobility Shift Assays – The PPARγ and RXRα proteins were expressed using coupled *in vitro* transcription and translation (TNT, Promega). EMSAs were performed using the [α-^{33}P]dATP labeled DR1 oligonucleotides (5'-AAACTAGGTCAAAGGTCA-3') as previously described [2 3]. The DR1 oligonucleotides utilized in the EMSA are identical to that used in the crystallography studies. Expression of wild type and mutant PPARγ were equivalent as determined by a western blot. A single band was detected for both wild type and mutant PPARγ proteins were detected using PPARγ antibody (ab27450, Abcam). For the supershift assay, PPARγ antibody (ab27450, Abcam) or RXRαantibody (sc-774, Santa Cruz) was used to confirm the identity of the protein within the gel.

Table S1. Data collection and refinement statistics.

Data collection and refinement statistics

	Rosiglitazone	BVT.13	GW9662
Data collection			
Space group	$P2_1$	P1	$P2_1$
Cell dimensions			
a, *b*, *c* (Å)	63.80, 146.51, 67.22	64.19, 66.91, 78.46	63.59, 146.78, 67.23
α, β, γ (°)	90, 115.59, 90	70.95, 82.56, 62.88	90, 115.52, 90
Wavelength	0.97945	1.00000	1.00000
Resolution (Å)	50-3.1 (3.21-3.10) *	50-3.2 (3.26-3.20)	50-3.1 (3.21-3.10)
R_{sym} or R_{merge}	9.9 (36.8)	6.4 (11.5)	9.7 (48.6)
$I/\sigma I$	13.42 (1.83)	17.15 (5.28)	13.2 (1.8)
Completeness (%)	99.1 (96.2)	92.3 (68.7)	98.8 (90.1)
Redundancy	3.1 (2.7)	2.1 (1.6)	3.8 (3.0)
Refinement			
Resolution (Å)	46.71-3.1 (3.29-3.1)	38.93-3.2 (3.4-3.2)	46.76-3.1 (3.29-3.1)
No. reflections	36204	16543	18669
R_{work}/ R_{free}	0.213/0.268 (0.348/0.383)	0.201/0.272 (0.208/0.282)	0.214/0.276 (0.340/0.418)
No. atoms			
Protein/peptide	5408	5340	5387
DNA	814	814	814
B-factors			
Protein/peptide	78.941	84.211	89.421
DNA	68.228	69.47	81.995
R.m.s deviations			
Bond lengths (Å)	0.007	0.007	0.007
Bond angles (°)	1.3	1.3	1.3

*Highest resolution shell is shown in parenthesis. Standard definitions were used for all parameters [4]. Data for limiting resolution shells is in parentheses. Data collection and refinement statistics come from HKL-3000 [5].

Table S2. Human PPARγ missense mutations in DBD or LBD associated with partial lipodystrophy, dyslipidaemia and insulin resistance [6 7 8] or colon cancer [9]

Mutation	Disruptive effect
C114R (DBD)	Prevents Zn nucleation, DBD folding, DNA binding
C131Y (DBD)	Prevents Zn nucleation, DBD folding, DNA binding
C162W (DBD)	Prevents Zn nucleation, DBD folding, DNA binding
P115Q (DBD)	Impacts the adjacent Zn-coordinating residue
V290M (LBD, helix 3)	Located within ligand binding pocket, alters contact to ligands and to the coactivator docking residue S289
F360L (LBD, loop b/w H6 t& H7)	Not known
R397C (LBD, loop b/w H8 & H9)	Disrupts salt bridge to E324 of helix 5 and van der Waals interaction with Y477 of helix 12
P467L (LBD, helix 12)	Effects on helix-12 and its activation function
Q286P (LBD, helix 3)	Located within ligand binding pocket, alters contacts to ligands
R288H (LBD, helix 3)	Located within ligand binding pocket, alters contacts to ligands

Additional mutations in the A/B region were not included due to lack of structural visualization.

Figure S1

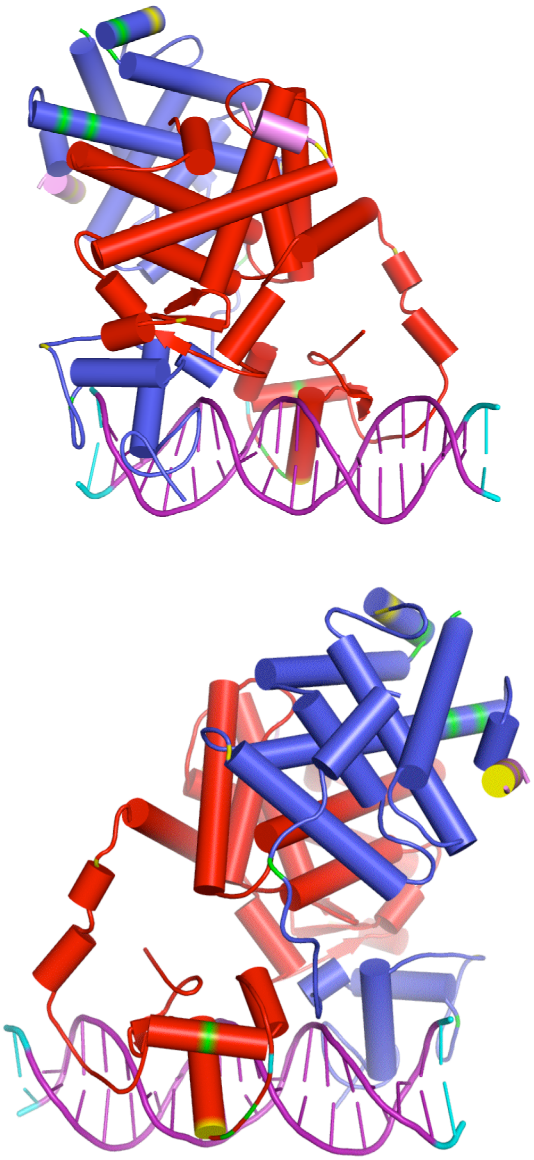

Figure S1. 180-degree views of the complex showing the sites of crystal lattice contacts in the P21 crystal lattice (rosliglitzone and GW9662 complexes) and P1 crystal lattice (BVT.13 complex). PPARγ is red, RXRα is blue, DNA is purple and coactivator peptides are magenta. Yellow and green surfaces on the proteins show the distinct contact sites in the P1 and P21 crystal forms, respectively. Cyan shows the DNA duplex ends, which participate in crystal packing in both crystal forms.

Figure S2

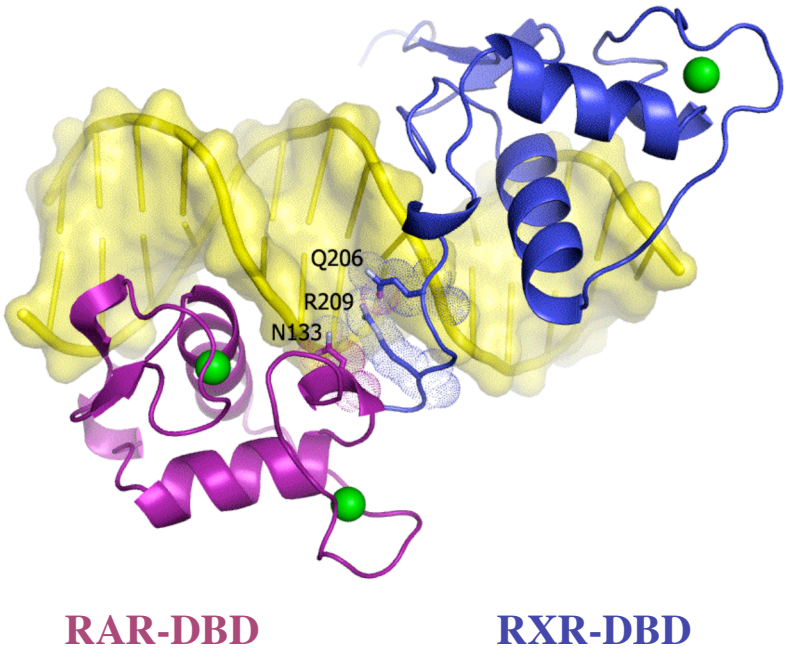

Figure S2. Similarity of the RARα-RXRα DBD heterodimer with that of the PPARγ-RXRα heterodimer at their DBD-DBD interfaces (see Figure 2B). In both heterodimers, RXRα uses Gln-206 and Arg-209 to form its DNA dependent contacts, while PPARγ and RARα each use identically positioned asparagines (Asn-160 from PPAR, Asn-133 from RAR). Both heterodimers also use the DNA minor groove of the lone spacer for their interactions..

Figure S3

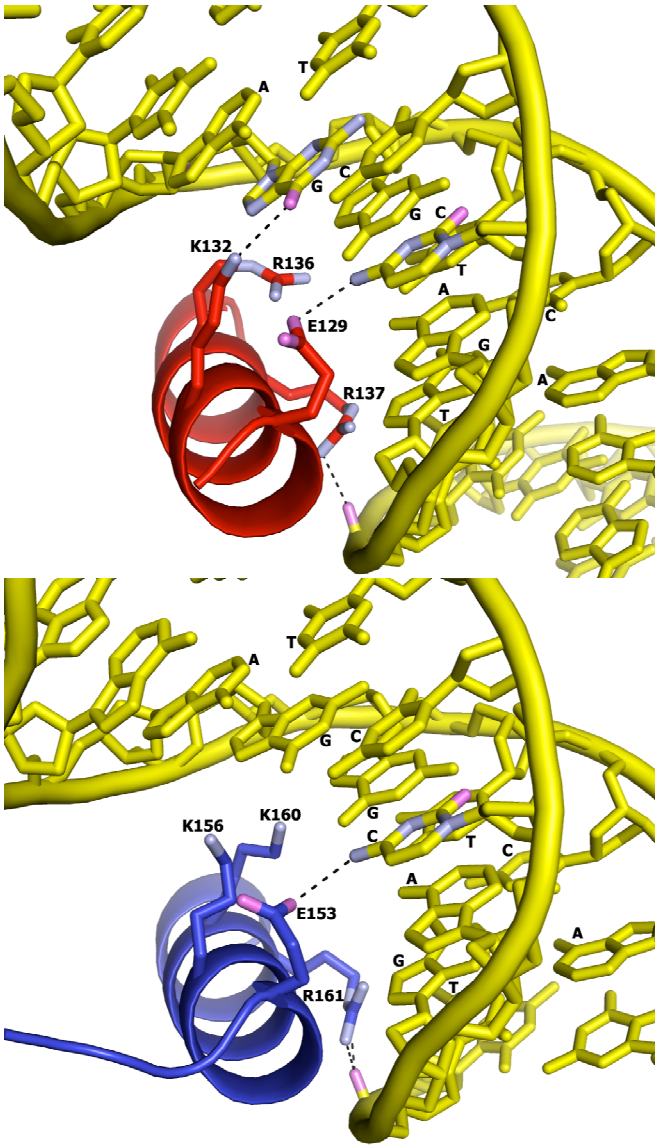

Figure S3. The base-specific contacts of the recognition alpha helix from PPARγ (red) and RXRα (blue) with their AGGTCA half-sites.

Figure S4

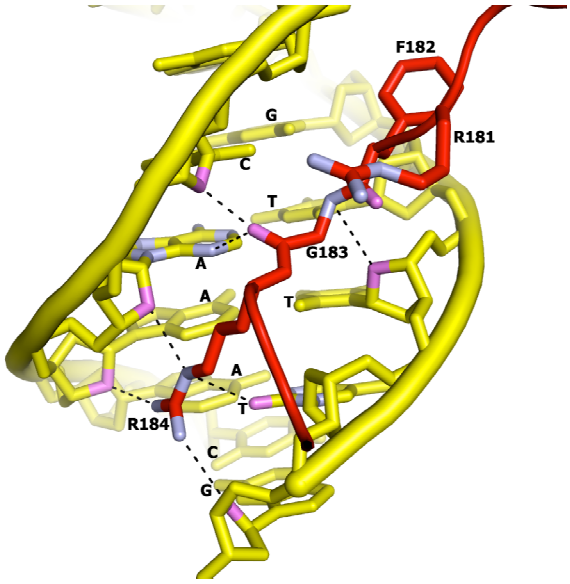

Figure S4. The interactions of the PPARγ hinge region with the AAACT element preceding the DR1.

Figure S5

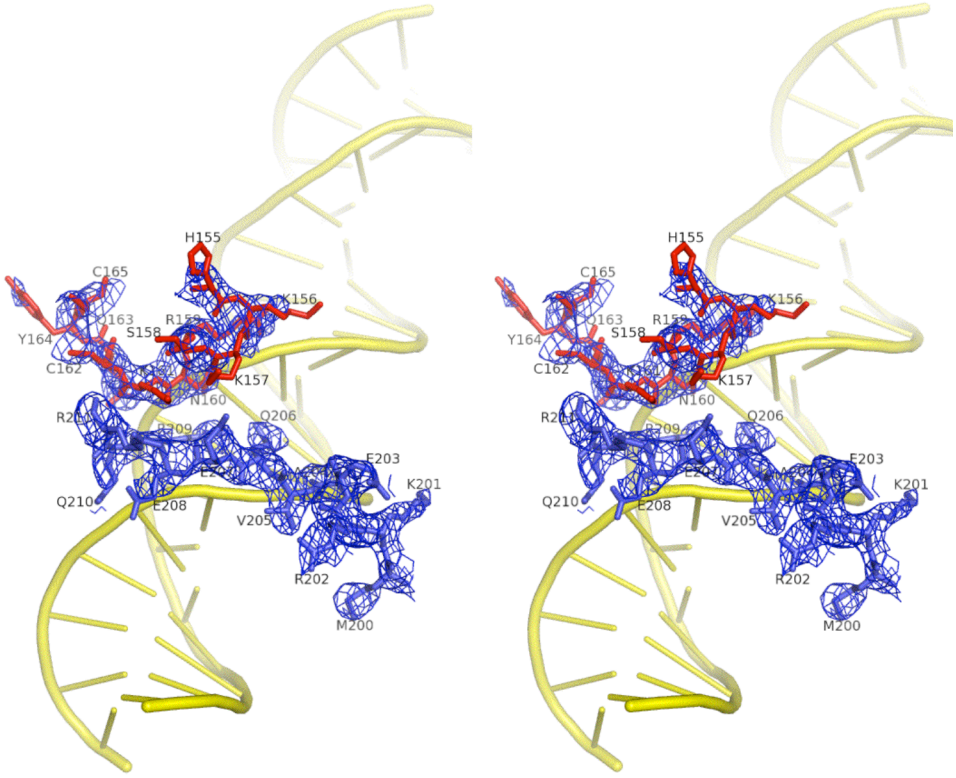

Figure S5. Stereoview, composite omit 2fo-fc electron density, showing the DBD-DBD interface. PPARγ is red, RXRα is blue.

Figure S6

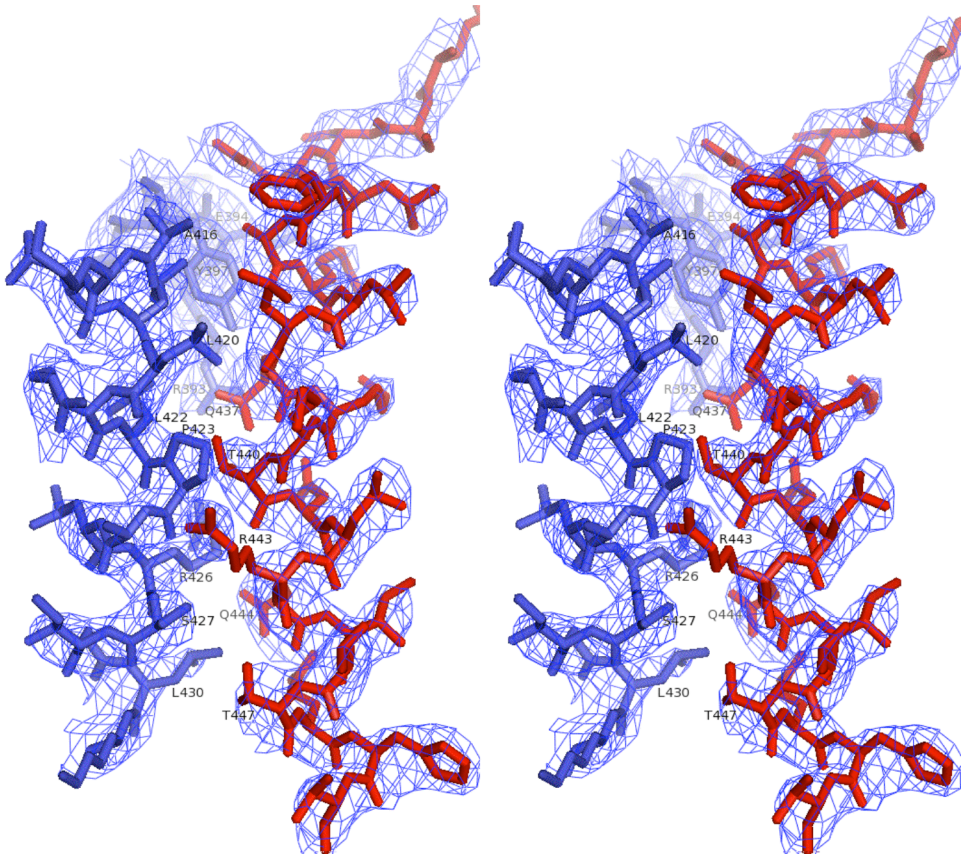

Figure S6. Stereoview, composite omit 2fo-fc electron density, showing part of the LBD-LBD interface. PPARγ is red, RXRα is blue.

Figure S7

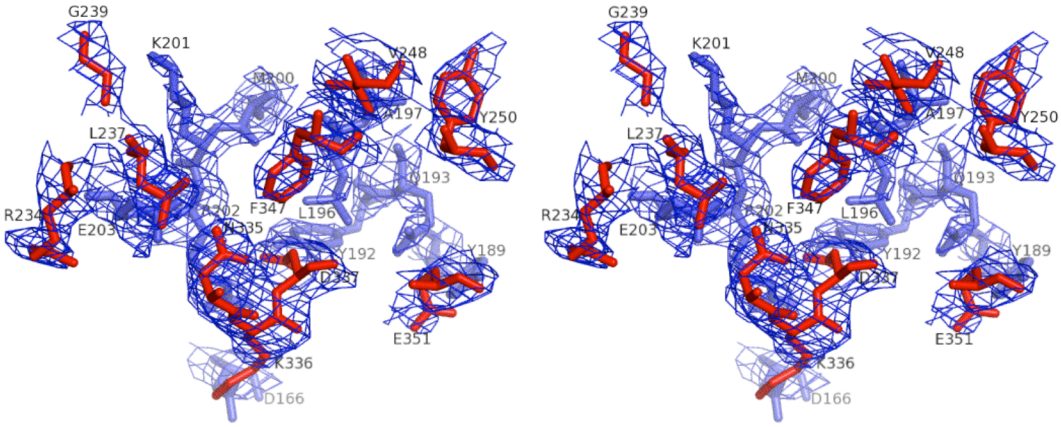

Figure S7. Stereoview, composite omit 2fo-fc electron density, showing the PPARγ - LBD interface with the RXRα-DBD. PPARγ is red, RXRα is blue.

Figure S8

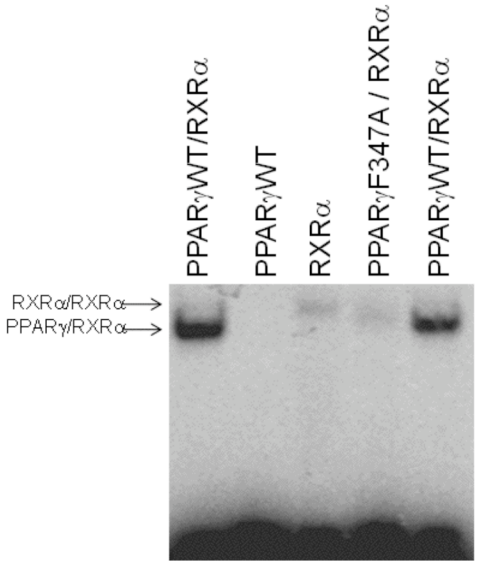

Figure S8. Electrophoretic mobility shift assay (EMSA) showing the binding of PPARγ, RXRα and their combination on PPRE DNA. A F347-A mutant within the LBD of PPARγ impacts the PPRE binding ability of the complex. A small amount of RXRα homodimers is noted when only RXRα interacts with the DR1 PPRE; however only the PPARγ/RXRα heterodimer band is noted when both receptors are included. The identities of the bands are confirmed in Figure S9. The PPARγ WT and F347A mutant were expressed at similar levels.

Figure S9

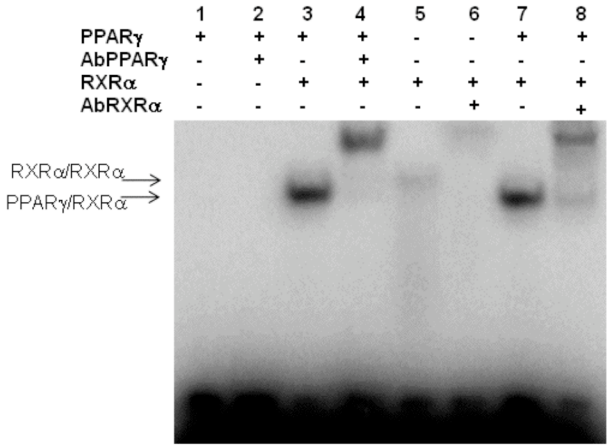

Figure S9. The use of specific antibodies to confirm the presence of receptors associated with EMSA shifted bands. The PPARγ/RXRα heterodimer is recognized and retarded by either the PPARγ or RXRα antibodies. The light RXRα homodimer band is recognized and retarded by the RXRα antibody.

Figure S10

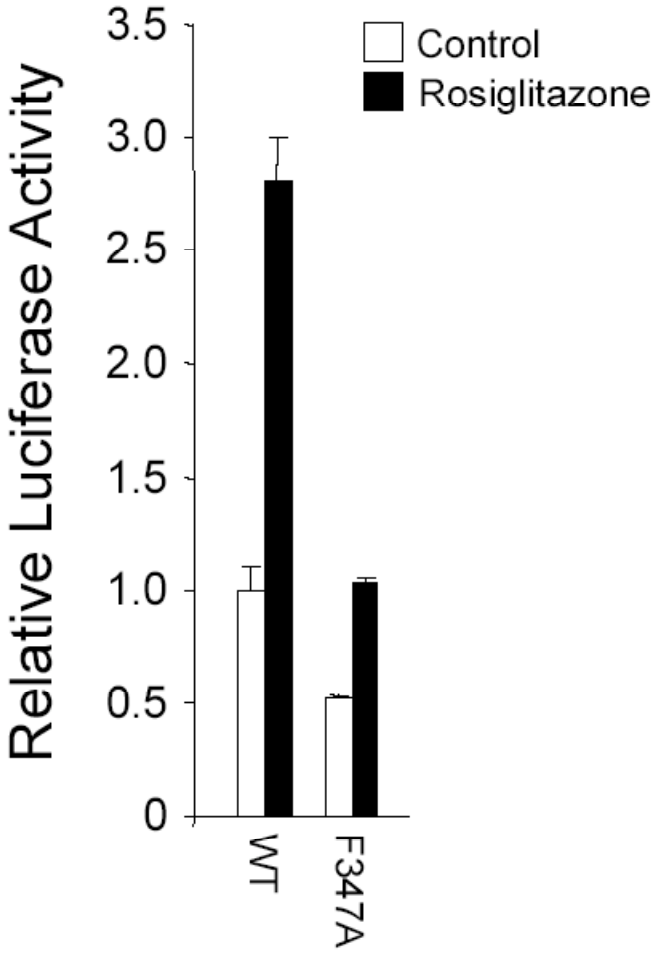

Figure S10. Luciferase reporter data showing that the F347A mutation in the PPARγ-LBD prevents the ability of the PPARγ-RXRα complex to stimulate gene expression.

Figure S11

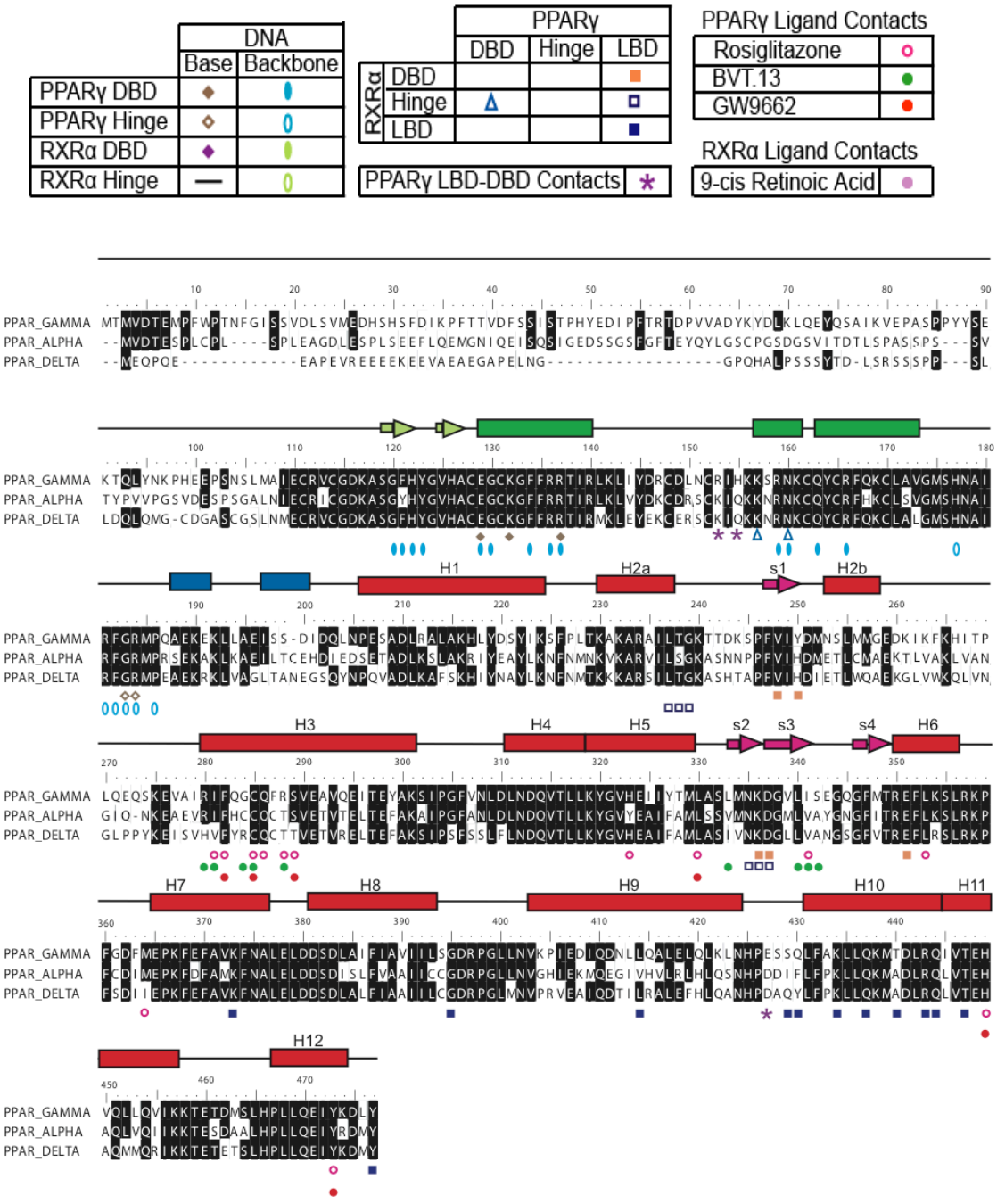

Figure S11. Sequence alignment of the PPAR family of nuclear receptors. Symbols on top indicate the different types of interactions along observed along the PPARγ polypeptide. Green, blue and red segments correspond to the DBD, hinge and LBD regions, respectively. All marks indicated interactions distances consistent with hydrogen –bonding and van der Waals interactions.

Figure S12

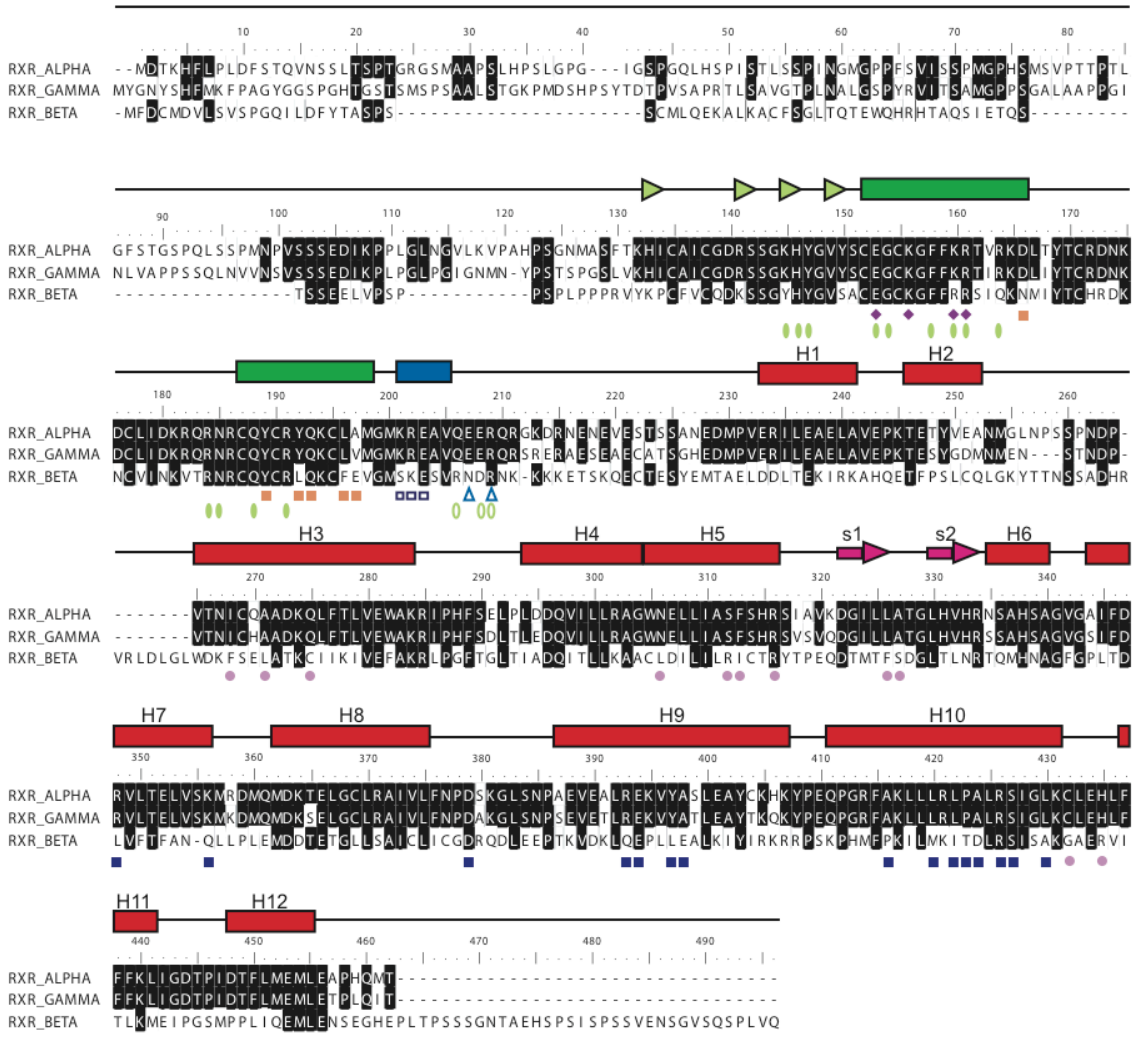

Figure S12. Sequence alignment of the RXR family. Symbols and segment colors are as indicated in Figure S10.

Figure S13

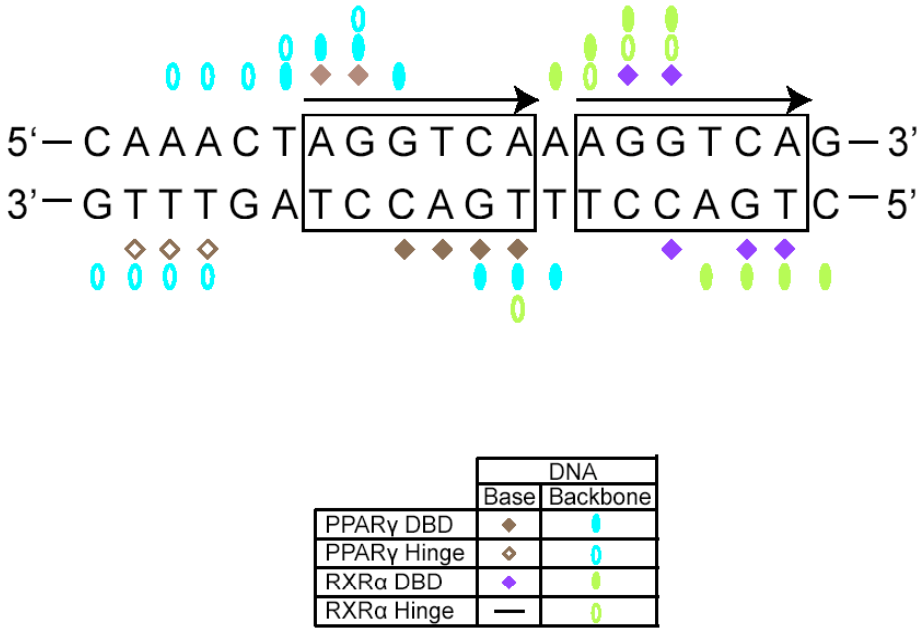

Figure S13. The observed footprint of RXR an PPAR proteins on the PPRE. Symbols are described on lower panel.

Supplementary References

1. Forman, B. M. et al. Androstane metabolites bind to and deactivate the nuclear receptor CAR-beta. *Nature* **395**, 612-5 (1998).
2. Burris, T. P., Guo, W., Le, T. & McCabe, E. R. Identification of a putative steroidogenic factor-1 response element in the DAX-1 promoter. *Biochem Biophys Res Commun* **214**, 576-81 (1995).
3. Stayrook, K. R. et al. Regulation of human 3 alpha-hydroxysteroid dehydrogenase (AKR1C4) expression by the liver X receptor alpha. *Mol Pharmacol* **73**, 607-12 (2008).
4. Drenth, J. *Principles of protein x-ray crytallography*. (Springer-Verlag, New York, 1994).
5. Minor, W., Cymborowski, M., Otwinowski, Z. & Chruszcz, M. HKL-3000: the integration of data reduction and structure solution--from diffraction images to an initial model in minutes. *Acta Crystallogr D Biol Crystallogr* **62**, 859-66 (2006).
6. Savage, D. B. PPAR gamma as a metabolic regulator: insights from genomics and pharmacology. *Expert Rev Mol Med* **7**, 1-16 (2005).
7. Agostini, M. et al. Non-DNA binding, dominant-negative, human PPARgamma mutations cause lipodystrophic insulin resistance. *Cell Metab* **4**, 303-11 (2006).
8. Semple, R. K., Chatterjee, V. K. & O'Rahilly, S. PPAR gamma and human metabolic disease. *J Clin Invest* **116**, 581-9 (2006).
9. Sarraf, P. et al. Loss-of-function mutations in PPAR gamma associated with human colon cancer. *Mol Cell* **3**, 799-804 (1999).